Modelling of Strain-Rate Dependence of Deformation and Damage Behavior of HSS- and UHSS at Different Loading States

Andreas Trondl[1], Dong-Zhi Sun[1]

[1]Fraunhofer Institute for Mechanics of Materials IWM

1 Abstract

The predictive capability of crash simulation concerning material failure is still in need of improvement due to the coupled complex influences of triaxiality, strain rate and temperature. Because of their lower ductility the use of high- and ultra-high strength steels (HSS&UHSS) requires a more accurate prediction of failure. This subject commonly leads to more complicated material- and failure models to describe complex interactions between deformation, strain rate and temperature, which usually results in longer computational time. On the other hand, due to the high complexity of crash simulation structures, simpler and less time-consuming material models and numerical methods are required to keep simulation times in an acceptable frame. For this reasons, a material model which considers the influences of strain rates and adiabatic effects was suggested and applied to simulate different testing scenarios. To avoid the time-consuming fully coupled thermal-mechanical approach, a strain-rate dependent Taylor-Quinney-Coefficient was introduced to control local adiabatic heating which lead to variable softening effects for different strain rates. Additionally, numerical investigations on the GISSMO damage model were carried out. Influences of the stress state (triaxility) and strain rate on the failure behavior of HSS&UHSS were characterized and simulated. To demonstrate the capabilities of the used approaches, loading tests on different geometries of specimens e.g. tension, shear tension, notch tension, pierced tension and Nakajima specimens were conducted with optical and infrared measurement of local strain and temperature fields. Especially the adiabatic softening and the change of failure strain at higher strain rates under different stress traxialities were analyzed.

KEYWORDS: deformation behavior, failure behavior, plasticity model, triaxiality, GISSMO, UHSS, HSS, 22MnB5, HX340LAD, Taylor-Quinney-Coefficient, failure line, adiabatic, thermo-mechanical effects, strain rate

2 Introduction

In the trend of lightweight construction more and more HSS&UHSS come to application in automotive structural components. Since the ductility of HSS&UHSS is relatively low, damage behavior of these materials has to be modelled in vehicle crash simulations to achieve a reliable crash worthiness prediction. However, the predictability of damage behavior under crash loading is still in need of improvement, since the influences of stress state, strain rate and temperature on damage development are very complex and no efficient and reliable numerical methods are available for damage modeling in crash simulation.

Until now most experimental results about the influence of stress triaxiality on failure behavior are achieved under static loading [1, 2, 3]. The main points of these investigations lie on the realization of different stress states for material characterization e.g. from pure shear over uniaxial tension, plane strain to biaxial tension. Based on the systematic experimental investigations different microscopic mechanisms of ductile failure like dimple fracture and shear fracture are recognized and the corresponding damage criteria are derived [4, 5, 6]. There are only a few publications about the influence of both stress state and strain rate on damage behavior [7, 8]. As the experimental tests at high strain rates are complex and need special facilities, the strain-rate dependence of failure strain is usually characterized only using smooth tension specimens. Dynamic tests under multi-axial loading especially under shear loading are missing. During dynamic testing not only the higher strain rate but also the temperature rise converted from plastic work (adiabatic heating) affect the deformation and damage behavior of material. However, there are no systematic investigations about the influence of strain rate and adiabatic heating on localization and damage behavior in different specimen tests.

The use of a suitable material model taking into account strain rate and temperature effects is essential for damage modeling since nearly all damage criteria for ductile rupture are based on local plastic strain and triaxiality which depend strongly on strain rate and temperature. A lot of material

models for description of strain rate effects are available for crash simulations. While Cowper and Symonds [9] and Johnson and Cook [10] used empirical models with a multiplicative law for strain rate dependence, Macherauch and Vöhringer [11] suggested a theoretic model with an additive law for a thermic and non-thermic contribution to the flow stress. The temperature rise during a dynamic tension test depends on plastic deformation and strain rate. In the case that the critical velocity for the adiabatic condition is reached, the temperature rise can be easily calculated from the relationship to the plastic energy. If a strain rate is lower than the critical value for the adiabatic condition, heat transportation has to be considered for the calculation of temperature change. Since no thermo-mechanical coupling is used in normal crash simulations, a simple solution for calculation of the temperature rise at different strain rates is required. An interesting method based on a strain-rate dependent factor (Taylor-Quinney coefficient) was used in [12]. However it is not clear how the factor is affected by specimen geometry and especially by strain gradients. The failure models used for crash simulations are mainly empirical models since micromechanical damage models like the Gurson model [13] describe only dimple fracture and are not applicable for shear rupture. The extended micromechanical models [14] contain also empirical parts and therefore are not more beneficial for applications. The basic idea of the available empirical failure models like Johnson-Cook [10], GISSMO [4], Bi-Failure [2], CrachFEM [15] and Bai-Wierzbicki [5, 16] is that ductile fracture is controlled by a fracture strain which depends on stress state which is characterized with triaxiality or in combination with a second parameter like Lode angle or shear stress ratio. For application of the failure models different specimen tests at different stress states are required to determine the corresponding damage curves by inverse simulations. The local fracture strains can be determined using digital image correlation (DIC) like ARAMIS. The open question is how the damage curves are influenced by strain rate. In this work the deformation and damage behavior of different steels for automotive application were characterized under multiaxial crash loading and modelled with an efficient method. The experimental tests at different stress triaxialities were performed with strain field measurements using high-speed cameras and with temperature measurement using an infrared high-speed camera [19], [20]. The micro-mechanisms of damage under different strain rates and triaxialities were analyzed by fractography and metallography. A simple numerical method for modeling the influences of strain rate and temperature on the flow behavior was used for crash simulations. The applied damage model was calibrated and verified by simulating the selected specimens under different stress states and strain rates.

3 Material and Damage Models

To describe the material behaviors sufficiently enough, a modelling approach based on deformation mechanisms is needed. An appropriate choice leads to use a strain rate dependent plasticity model for describing the deformation behavior and an additional damage model to depict the final failure of the material. Both models could be coupled or not, which leads to a more smooth or abrupt strain-stress characteristic of simulated specimens.

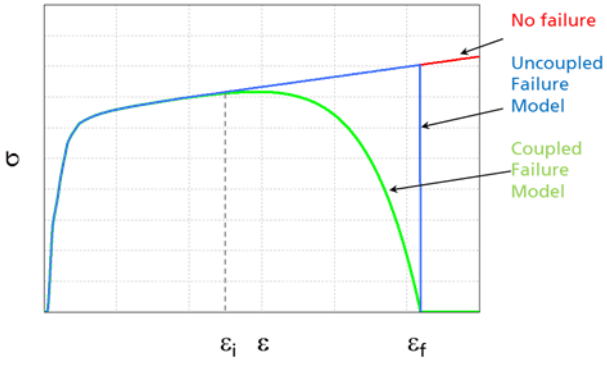

Fig.1: Deformation characteristics for different couplings between plasticity-, damage and failure models. (σ: stress, ε: strain, ε_i: strain at damage initiation, ε_f: failure strain)

The requirement for coupling the plasticity and damage model depends on the material. For example, UHSS show a small ductility and fail instantaneously, which often needs no coupling. On the other hand the failure behavior of more ductile steels is often smeared and smooth, which suggests a coupling of the plasticity and damage model. But coupling has one significant and practical disadvantage, because the calculated damage evolution changes strongly the deformation behavior before failure and makes the inverse simulation for the determination of true stress vs. true strain

curves more difficult. Therefore it is often more convenient to skip coupling, except for the case that the material characteristic really needs such approach.

3.1 Models for Strain-Rate and Temperature Dependence

The basic ingredient to describe the pre-fracture deformation behavior accurately is the proper choice of a suitable plasticity model. If the chosen material model is not suitable, the calibration of the material parameters in relation to the measurements can be principally carried out, but is not reliable for all different stress states (e.g. under tension, shear tension, biaxial tension, etc.). It is commonly known that local heating effects occur during high speed loading, which is mostly the case during crash relevant scenarios. This effect is significantly more pronounced for higher loading speeds. The reason of this fact lies in the conversion from the work of plastic deformation

$$\dot{W}_{pl} = \sigma\dot{\varepsilon}_{pl} \Rightarrow dW_{pl} = \sigma\left(\varepsilon_{pl}, \dot{\varepsilon}_{pl}, T\right)\dot{\varepsilon}_{pl}dt \tag{1}$$

to thermal energy

$$\dot{q} = \beta\dot{W}_{pl} \Rightarrow dq = \beta\sigma\left(\varepsilon_{pl}, \dot{\varepsilon}_{pl}, T\right)\dot{\varepsilon}_{pl}dt \tag{2}$$

which can be described by the Taylor-Quinney coefficient β [17]. The Taylor-Quinney coefficient in equation (2) is a constant material parameter and has the typical value of 0.9 for steels. The heat increase is primarily determined from the available time to conduct the generated heat (2) and the heat conduction behavior (3) which is mainly determined by the heat conduction coefficient λ

$$\dot{q} = \frac{\partial q}{\partial t} = -\lambda\frac{\partial T}{\partial x} \tag{3}$$

It is obvious that the available time for heat conduction decreases at higher strain rates, which leads to higher temperatures. In that case the heat conduction plays a negligible role and the local deformations run mainly under adiabatic conditions, which means no or remarkably reduced local heat exchange outwards is possible due to the short deformation time. On the other hand in case of lower strain rates the available time for heat conduction increases, which leads to a lower temperature rise, and non-adiabatic local deformation takes place. These mechanisms show the importance of heat conduction during plastic deformation at different strain rates. But for complex crash simulations in automotive applications it is not possible to take the heat conduction into account due to the time consuming thermo-mechanical coupled calculation. Therefore an applicable alternative solution is needed. First approaches to describe these circumstances are based on models of Johnson-Cook type

$$\sigma = \sigma_0\left(\varepsilon_p\right) \cdot f\left(\dot{\varepsilon}_p\right) \cdot g(T) \tag{4}$$

which use a multiplicative combination of the influences of plastic strain hardening $\sigma_0\left(\varepsilon_p\right)$ and strain-rate hardening $f\left(\dot{\varepsilon}_p\right)$ as well as temperature related softening $g(T)$. The calculation of the temperature field bases on the approach of Taylor-Quinney β (2) and the specific heat capacity c_p (5). Disadvantages of such models (4) are often the analytical approaches for $\sigma_0\left(\varepsilon_p\right)$, $f\left(\dot{\varepsilon}_p\right)$ and $g(T)$, which are inflexible and fit more or less only specific classes of materials. Additionally the multiplicative connection between $\sigma_0\left(\varepsilon_p\right)$, $f\left(\dot{\varepsilon}_p\right)$ and $g(T)$ given in (4) results in self-similarities of the described flow curves (yield surface), but strain rate hardening on different temperature levels is more complex [18].
The heating can be calculated from equation (2) and the specific heat capacity c_p by

$$dq = \rho c_p dT \Rightarrow dT = \frac{\beta}{\rho c_p}\sigma d\varepsilon = \frac{\beta}{\rho c_p}dW_{pl} \tag{5}$$

Due to the fact that the density ρ, the specific heat capacity c_p and the Taylor-Quinney coefficient β are constant quantities, it is obvious that the temperature rise is only determined by the increase of plastic work dW_{pl}. Therefore the temperature field in the model increases for non-adiabatic conditions unrealistically, because no heat conduction is considered in the model. This unrealistic temperature increase leads to over-pronounced thermal softening in the deformation behavior of the considered material for lower strain rates, where heat conduction becomes more important and non-adiabatic local deformations take place. To solve this problem a strain rate dependent Taylor-Quinney coefficient can be introduced. The main idea behind this approach is the reduction of the thermal heating at lower strain rates, which should compensate the not included heat conduction in the model. The main requirements of a strain-rate dependent function for the variable Taylor-Quinney coefficient are given below:

- The reduction of heat generation for lower strain rates should compensate the absence of heat conduction, which leads to a low value of β and non-adiabatic conditions
- Usual values of β (e.g. 0.9) for higher strain rates should describe sufficiently the adiabatic conditions
- For medium strain rates a suitable change of β should describe the non-adiabatic - adiabatic transition

Out of these requirements one suggestion of the strain-rate dependent Taylor-Quinney coefficient is given in the following equation (6)

$$\beta = \beta_0 \cdot \left[\frac{1}{2} + arctan\left(b_\omega \cdot ln\frac{\dot{\varepsilon}_p}{\dot{\varepsilon}_{p,\omega}}\right) \cdot \frac{1}{\pi}\right] \tag{6}$$

β_0 describes the Taylor-Quinney coefficient for adiabatic conditions which corresponds to the usual constant value from the literature (0.9). $\dot{\varepsilon}_{p,\omega}$ describes the strain rate for non-adiabatic – adiabatic transition. b_ω describes the width of the strain rate region where the non-adiabatic – adiabatic transition takes place. An exemplary shape of the approach (6) is given in (Fig. 2). It can be expected that unrealistic softening for lower strain rates will disappear, because the temperature evolution is considerably reduced in comparison to the standard model with a constant Taylor-Quinney coefficient (black and purple dashed lines in Fig. 3).

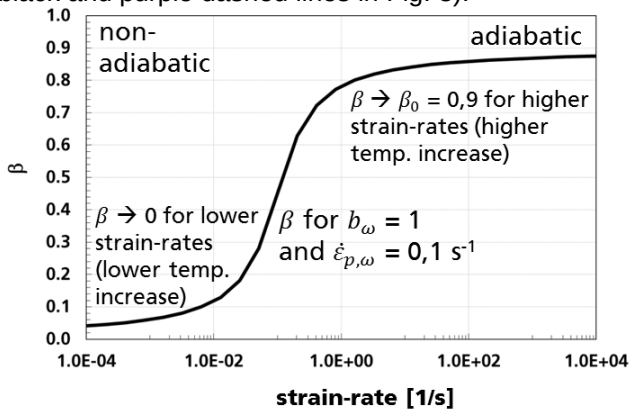

Fig.2: Strain-rate dependent Taylor-Quinney coefficient.

The consideration of the strain-rate dependent Taylor-Quinney coefficient (6) in the standard Johnson-Cook Model (4) leads to much more realistic temperature evolutions for lower deformation speeds. For higher strain rates the thermal behavior still shows adiabatic deformation.

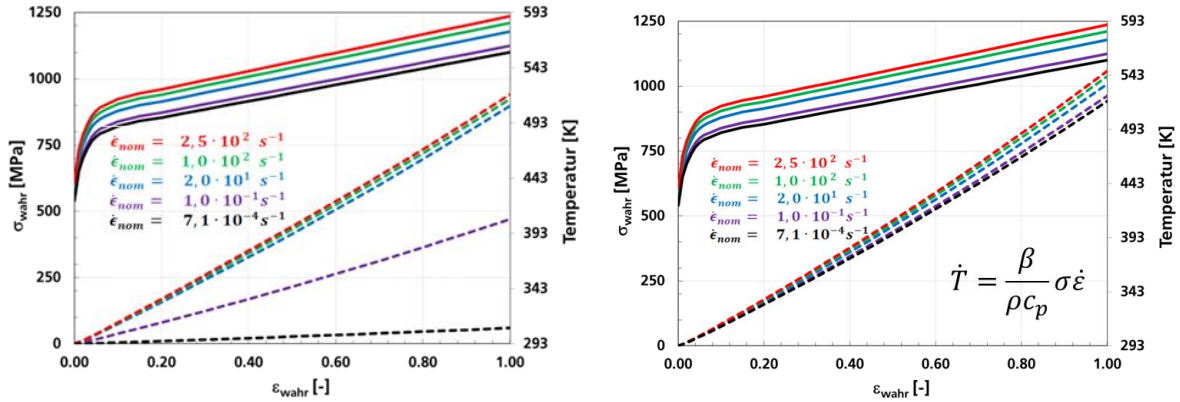

Fig.3: Temperature development for different strain rates in a standard plasticity model of Johnson-Cook type with variable Taylor-Quinney-coefficient left (solid lines: yield stress; dashed lines: temperature; different colors: strain rates) and constant Taylor-Quinney-coefficient right

3.2 Damage Model

The used approach for describing failure bases on a scalar damage parameter D which can be coupled or not to the actual stress state of the applied plasticity model. Fracture occurs when the cumulative scalar damage parameter D defined by (7) reaches the critical value of one

$$\tilde{\sigma}_{ij} = \frac{\sigma_{ij}}{1-D} \tag{7}$$

where σ_{ij} represents the Cauchy-stress for the undamaged and $\tilde{\sigma}_{ij}$ the Cauchy-stress for the damaged state. Johnson-Cook [10] proposed a linear damage accumulation. A more general non-linear damage accumulation is used here:

$$\frac{dD}{dt} = \frac{n}{\varepsilon_{pl,f}} \cdot D^{1-\frac{1}{n}} \cdot \frac{d\varepsilon_{pl}}{dt} \tag{8}$$

ε_p denotes the equivalent plastic strain and the exponent n is a parameter controlling the speed of growth in the damage evolution. $\varepsilon_{pl,f}$ denotes the local failure strain, which depends on the triaxiality η and is given by the failure curve $\varepsilon_{pl,f} := \hat{\varepsilon}_{pl,f}(\eta)$. From the definition of the triaxiality

$$\eta = \frac{\sigma_h}{\sigma_{vm}} \quad \sigma_h := \frac{1}{3}\sigma_{ii} \quad \sigma_{vm} := \sqrt{\frac{3}{2}\sigma_{ij}\sigma_{ij}} \tag{9}$$

it is clear that the local failure strain $\varepsilon_{p,f}$ depends on the stress state (hydrostatic stress σ_h, equivalent von Mises stress σ_{vm}), which is determined by the local strains and strain rates too $\varepsilon_{p,f} := \tilde{\varepsilon}_{pl,f}(\eta, \dot{\varepsilon}_{pl})$. Therefore it is obviously, that the development of damage variable D (8) depends strongly on the local deformation state (lower failure strain leads to faster damaging and higher failure strain results in slower damaging). The adjustment of most failure models based presently only on the failure behaviour for quasistatic loading conditions, which means for different strain rates no change of the failure curve is assumed. There are also approaches of self-similar scaling proposed which multiplies the quasistatic failure curve with a factor in dependency of strain rate. Additional approaches suggested for different strain rates a local scaling of the (quasistaic) failure behaviour for shear or biaxial dominant deformation states. But it is clear, the shape and the level of the failure curve changes with the local strain rates in a more general way. The investigation of this behaviour is one important part of this work.
For proportional loading the integration of (8) under the condition of Johnson-Cook damaging ($n = 1$) leads to $D = \varepsilon_p / \varepsilon_{p,f}$. From a physical point of view a non-linear evolution of damage is reasonable. However, the determination of the n-value is difficult. For this reason $n = 1.5$ was used in this work. To reduce the complexity during fitting the whole material model, no coupling of the scalar damage variable to the current stress states was assumed. For this approach, the evolution of the damage parameter D is calculated as a function of plastic strain and triaxiality and element deletion is executed when D reaches the value of one.

4 Simulation of Specimen Tests

The fit of the material model was done for different types of specimens which cause different stress states (triaxialities). The shear tension test, the pierced-hole tension test, the smooth tension test and the notched tension test were simulated and compared to the test data under quasi-static and dynamic loading conditions (medium and high strain rate).

4.1 Numerical models

The main ingredient for the numerical model is the modification of the temperature evolution for a strain-rate dependent Taylor-Quinney coefficient. For an explicit FEM code this can be done by a modification of the incremental update for the temperature. From equations (2) and (5) follows:

$$c_p \rho dT = \beta\left(\dot{\varepsilon}_{pl}(t)\right)\sigma\left(\varepsilon_{pl}, \dot{\varepsilon}_{pl}, T\right)\dot{\varepsilon}_{pl}dt \tag{10}$$

A discretization from state i to state $i+1$ of equation (10) leads to

$$c_p \cdot \rho \cdot (T_{i+1} - T_i) = \beta\left(\dot{\varepsilon}_{pl,i}\right) \cdot \sigma\left(\varepsilon_{pl,i}, \dot{\varepsilon}_{pl,i}, T_i\right) \cdot \Delta\varepsilon_{pl,i} \tag{11}$$

from which the update (12) can be easily derived.

$$T_{i+1} = T_i + \frac{\beta(\dot{\varepsilon}_{pl,i})}{c_p \rho}\sigma_{pl,i}\Delta\varepsilon_{pl,i} \tag{12}$$

For the plasticity model a more generalized Johnson-Cook approach was used.

$$\sigma = s\left(\varepsilon_p, \dot{\varepsilon}_p\right) \cdot g(T) \tag{13}$$

This approach avoids self-similarities of the flow-curves for different strain rates, which leads to better approximations of the yield surface and the measured fracture strains respectively. Furthermore a choice of a physically reasonable temperature-softening $g(T)$ and a strain rate dependent Taylor-

Quinney coefficient is useful to fit the unknown function $s(\varepsilon_p, \dot{\varepsilon}_p)$ to the test data. The fit of $s(\varepsilon_p, \dot{\varepsilon}_p)$ was done for every known test data set (index k) at different strain rates $\dot{\varepsilon}_{p,k}$, which leads to the unknown approximations $s(\varepsilon_p, \dot{\varepsilon}_{p,k}) = s_k(\varepsilon_p)$ of the flow curves. The analytic approaches for the strain rate related flow curves $s_k(\varepsilon_p)$ base on a generalized Voce approximation

$$s_k(\varepsilon_p) = \sum_{j=1}^{n} a_{i,j}\left(1 - e^{-b_{i,j}\cdot\varepsilon_p}\right) \tag{14}$$

where $a_{k,j}$ and $b_{k,j}$ are fit parameters. The fit was done by using the optimization tool LS-Opt.
For a choice of a physically reasonable temperature softening $g(T)$ the commonly known analytical approach of Johnson-Cook

$$g(T) = 1 - \bar{T}^m \quad \bar{T} = \frac{T - T_R}{T_{MELT} - T_R} \tag{15}$$

does not lead to suitable results (especially for shear dominated stress states) because the decrease of thermal softening for higher temperatures is too strong (blue curve in Fig. 4).This circumstance is directly related to the strong localization during the shear tension test.

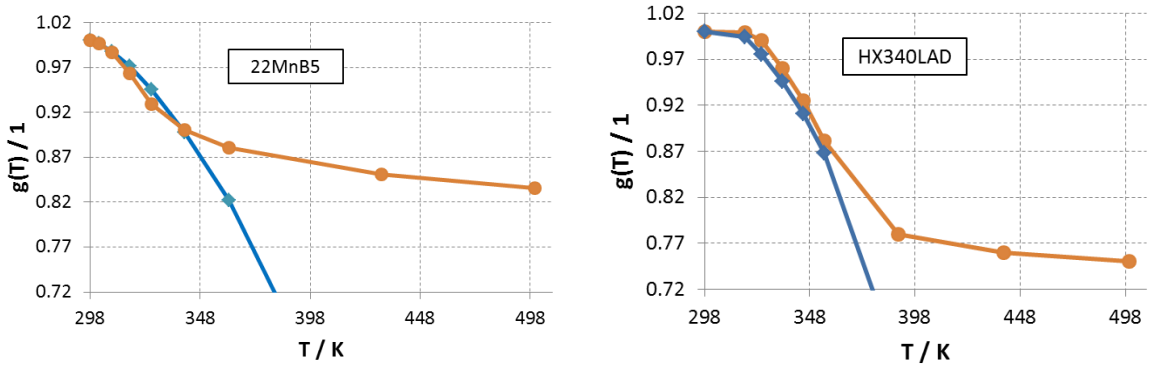

Fig.4: Thermal softening (blue curve: analytical Johnson-Cook approach (15); orange curve: physically reasonable choice)

Therefore a more realistic choice of $g(T)$ is required, which has to reduce the thermal softening for higher temperatures (orange curve in Fig. 4). With this choice of the thermal softening a good approximation for all different loading tests can be realized.

4.2 Comparison between Experiments and Simulations

To show the quality of the used model, verification for different stress states (triaxialities) was done. The dynamic experiments were carried out by means of high speed testing equipment [19]. The determination of the local specimen elongations until fracture was done by optical measurement of applied speckle patterns with high-resolution high-speed video cameras (grey scale value correlation [20], [22]).

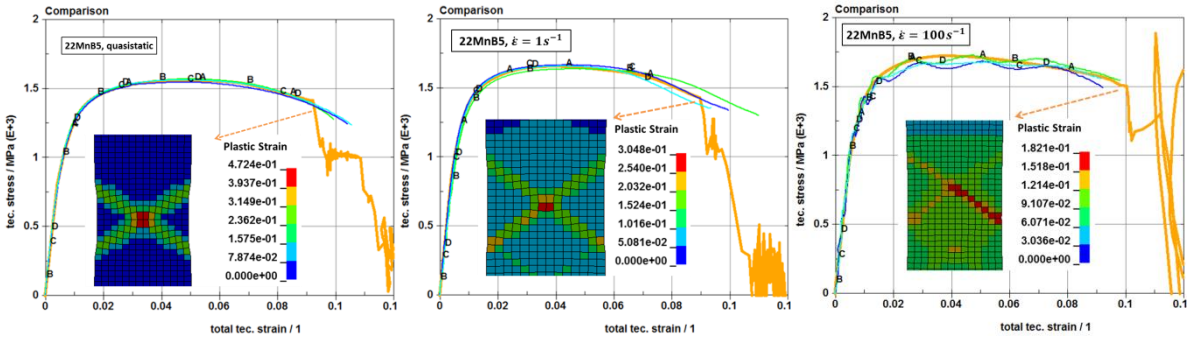

Fig.5: Comparison between simulation (thick orange lines) and experiment (thin colored green, blue and cyan lines) of strain vs. stress curves for the tension tests under three different strain rates for 22MnB5

The determination of thermal effects has been carried out by using high-speed infrared camera equipment, which was individually calibrated for the different test series and specimen shapes [21]. The verifications demonstrate a good agreement with experiments in the global (force-displacement) measurements. The investigated loading speeds reached from quasistatic (nominal strain rate for

tension 0.001/s) over medium strain rates (1/s) up to high speeds (nominal strain rate for tension 100/s). The following figures show the good agreement to the related test data of the 22MnB5 under different loading and deformation conditions. From Fig. 5 one can see clearly a significant less pronounced localization for the high strain rate (Fig. 5 right) in comparison to the medium strain rate (Fig. 5 middle) and the quasistatic load case (Fig. 5 left).

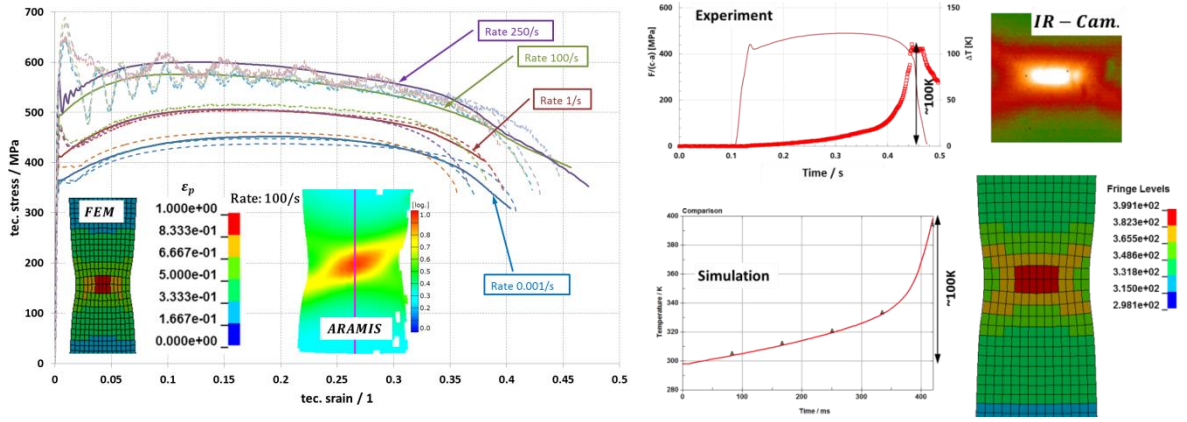

Fig.6: left: Comparison between simulation (solid lines) and experiment (dashed lines) of strain vs. stress curves for the tension tests under four different strain rates and an exemplary local plastic strain field at high strain rate (100/s) for a ductile HX340LAD
right: Comparison between simulation (below) and experiment (top) of temperature development and local temperature field for medium strain-rate of 1/s (tension test) HX340LAD

This fact leads to lower failure strains for tension-dominated load cases in relation to rising strain rates for the UHSS 22MnB5. The less pronounced necking of the UHSS 22MnB5 in comparison to the more ductile HX340LAD (Fig. 6 left) is also well describable for all observed and simulated strain rates.

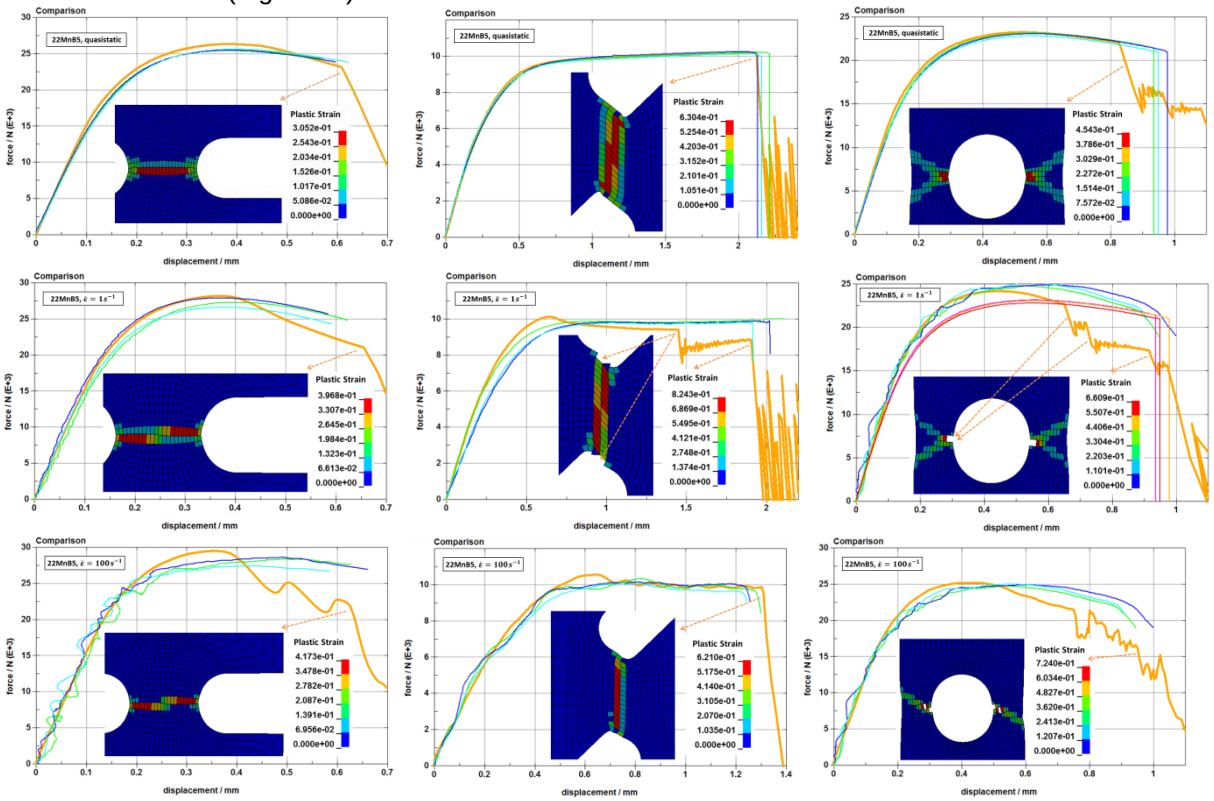

Fig.7: Comparison between simulation (thick orange line) and experiments (thin colored lines) of force-displacement curves and simulated local strain field for strain rates from 0.001/s (first row) to 1/s (second row) up to 100/s (third row) for 22MnB5

Both materials (less ductile UHSS 22MnB5 and more ductile HX340LAD) shown in the simulation under quasistatic loading an expected minor temperature evolution (<10K) during the strong

localization at the end of the tests, which is related to the influence of the strain-rate dependent Taylor-Quinney coefficient.
For the medium (1/s) and higher strain rate (100/s) significant thermal effects can be observed in experiment and in the simulation as well, which is exemplarily shown in Fig. 6 right. Additionally for higher strain rates (100/s) a more pronounced temperature increase is expected and is confirmed by the experimental observation and the simulation results.
The deformation characteristics for other stress states (triaxialities) at different strain rates (0.001/s up to 100/s) fit the experimental observations also well. To induce the different stress states (triaxialities) varied specimen shapes are used, such like notched- and holed tensile specimen shapes but also slotted specimen shapes for shear dominant loadings and round sheets for Nakajima tests.

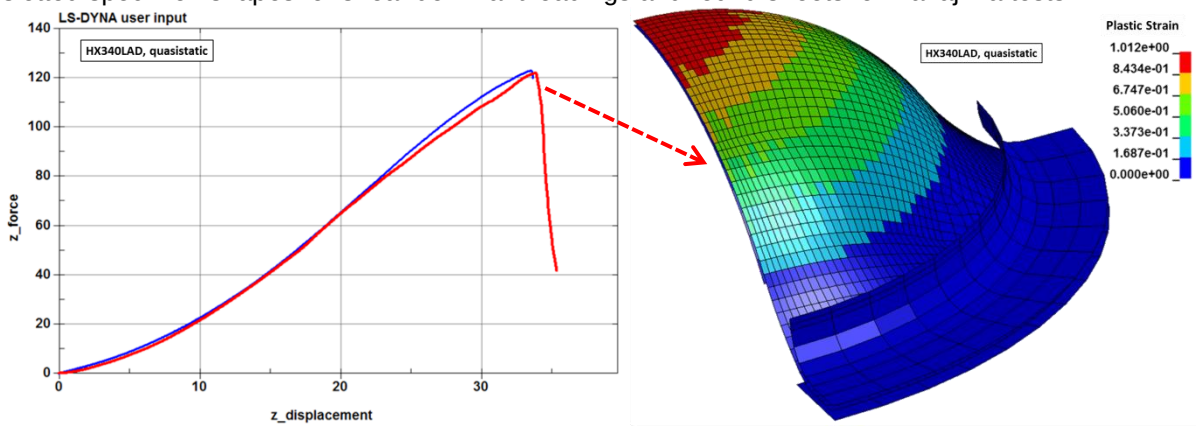

Fig.8: Comparison between simulation (thick red line) and experiment (thin blue line) of a force-displacement curve (left) and the simulated local strain field (right) for a Nakajima test under quasistatic loading (ductile micro-alloyed HX340LAD)

In contrast to all tension tests of the UHSS 22MnB5, the other specimens in Fig. 7 shown a similar localized distribution of the plastic strain field over all observed strain rates, which can be explained by the specimen's shape that enforces strain localization. For the notched- and holed tension test the absolute level of the plastic strains increases with higher strain rates (Fig. 7 left and right column). The plastic strain field for shear dominated deformations shows a notable increase from the quasistatic to the medium strain rates (1/s) and a decrease from the medium strain rates (1/s) up to higher strain rates (100/s), which can be seen in Fig. 7 (middle column). This fact has a direct influence on the failure behavior and results in an in- and decrease of the failure curve for smaller triaxialities.

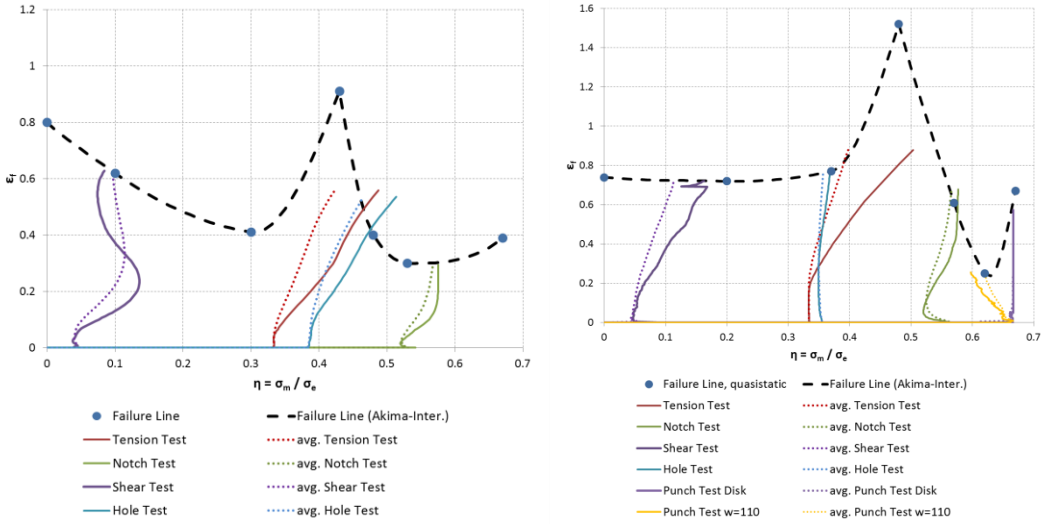

Fig.9: Quasistatic failure behavior for a UHSS 22MnB5 (left) and for comparison a ductile micro-alloyed HX340LAD (right)

The curves in Fig. 9 represent the failure line for quasistatic loading (thick black dashed lines) and the loading path (evolution of the equivalent plastic strain and triaxility respectively) of the first failing elements in relation to different tests, which are shown in Fig. 5 and 7. The calibration of the failure model represents a compromise of all different stress states (triaxialities). One problem in the

calibration is the interaction of the stress-state evolution between the pure tension- and the holed tension test. In principle, the first failing elements in both tests start at similar triaxialities levels of 1/3. But in case of the22MnB5 for the holed tensile test the maximum damage appears inside the root of the hole-notch, where triaxialities of 0.4 exist. This fact is related to the elastic-plastic behavior in opposite to pure elasticity, where the maximum damage is in the root of the hole notch. Therefore the dominant stress state for the holed tension tests has triaxialities between 0.4 and 0.55, which explains the shape of the failure curve in that interval. In addition, the calibrated failure lines for the medium (1/s) and higher strain rates show in principle similar distributions as in Fig. 9 and are used in all simulations of Fig. 7. For the ductile micro-alloyed HX340LAD the Nakajima test (Fig. 8) leads to a significant increasing of the failure strain under biaxial loadings, which represent triaxialities of 2/3.

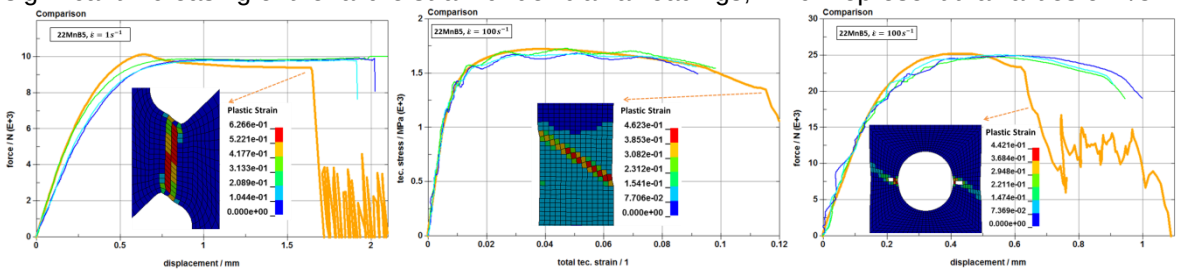

Fig.10: Exemplarily comparison between simulation (thick orange line) and experiments (thin colored lines) of force-displacement curves and simulated local strain field for shear tension test (left) at strain-rates of 1/s, tension (middle) and holed tension test (right) at strain rate of 100/s by using quasistatic failure curve

Comparisons of selected simulations (Fig. 10), which are related to different triaxialities, shown for medium and higher strain rates (1/s and 100/s) a less agreement to experimental results when the quasistatic failure curve is used (cp. Fig. 10 and Fig. 7). But there are also other cases in which the agreement between simulation and measurement is more or less acceptable when the failure curve of quasistatic case is used for other strain rates, especially in tension test under medium and shear tension test under high strain rate.
In addition it should be also mentioned, that the deformation behaviour for more localized and complex loadings, such as notched- and holed tension tests, is not very good approximated for higher strain rates (Fig. 7), which has an influence on the characteristic of the failure lines too. But the complexity for the constitutive models is limited in crash simulations, and under this condition the calibrated model fits quite well in comparison to other approaches. Furthermore, in the presented model calibrations no coupling between stress and damage evolution is used, which leads to non-smooth and abrupt discrete stepwise force- displacement characteristics, and influences the characteristic of the failure lines too.
Using different failure curves within a strain rate range leads in most load cases (triaxialities) to better agreements between simulations and experiments for the investigated 22MnB5 and HX340LAD. But on the other hand the calibration of the failure model for each strain rate is more time consuming.

5 Summary

The deformation and damage behavior of different steels for automotive application were investigated under multiaxial crash loading through various experiments and numerical simulations. A modified plasticity model was proposed to describe the temperature development for higher and lower strain rates in a sufficient manner without using the time consuming thermo-mechanical coupling, which is important for crash relevant applications. Several examples were presented to show the applicability of the model for different stress states. The comparisons of simulations to experimental investigations show good agreements for different triaxilities. A failure model and a coupling to the plasticity model were presented for the UHSS 22MnB5 and ductile micro-alloyed steel of type HX340LAD. The failure strain shows a significant increasing between triaxialities form 0.5 up to 0.67 for the ductile micro-alloyed steel HX340LAD. For shear dominated dynamic loadings decreasing failure strain with increasing strain rate was observed and verified in simulations. For tension dominated loadings a reduction of plastic failure strains is determined by the simulations, which can be explained by a more pronounced homogeneous plastic strain field for higher strain rates.

6 Acknowledgments

We thank the “Forschungsvereinigung der Arbeitsgemeinschaft der Eisen und Metall verarbeitenden Industrie e.V. (AVIF)” and the Research Association for Steel Application (FOSTA) as well as different industrial partners for funding this project.

7 Literature

[1] Bao, Y., Wierzbicki, T., On fracture locus in the equivalent strain and stress triaxiality space, Int. J. Mech. Sci., 2004, 46 (81), 81-98.
[2] Sun, D.-Z., Andrieux, F., Feucht, M., Damage modelling of a TRIP steel for integrated simulation from deep drawing to crash, 7th European LS-DYNA Conference, 14.-15. Mai 2009, Salzburg, (2009) B-III-04.
[3] Zhu, H., Zhu, L., Chen, J.H., Lv, X.-F., Investigation of fracture mechanism of 6063 aluminum alloy under different stress statesInt. J. Fract., 2007, 146, 159-172.
[4] Neukamm, F., Feucht, M., Haufe, A., Consistent damage modelling in the process chain of forming to crashworthiness simulations, 7. LS-DYNA Anwenderforum, 30. Sept.-1. Oct.2008 Bamberg.
[5] Bai, Y., Wierzbicki., T., A new model of metal plasticity and fracture with pressure and lode dependence. Int. J. Plast., 24(6) 2008, 1071 – 1096.
[6] Andrieux, F., Sun, D.-Z., Damage modelling for simulation of process chain from forming to crash, Int. J. Mat. Res. 2010, Vol. 101, 8, 963-971.
[7] Authenrieth, H., Schulze. V., Herzig, N., Meyer, L.W., Ductile failure model for the description of AISI 1045 behavior under different loading conditions, Mech. Time-Depend Mater (2009) 13: 215-231.
[9] Cowper, G. R., Symonds, P. S., Strain hardening and strain rate effects in the impact loading of canti-lever beams, Division of Applied Mathematics Report. Brown University, 28, 1957.
[10] G.R. Johnson, W.H. Cook, Fracture characteristics of three metals subjected to various strains, strain rates, temperatures and pressures, Engineering Fracture Mechanics, vol.21 (1985), No.1, pp.31-48.
[11] Macherauch, E., Vöhringer, O., Das Verhalten metallischer Werkstoffe unter mechanischer Beanspruchung, Z. Werkstofftechnik 9 (1978), 370-391.
[12] Hodowany, J., Ravichandran, G., Rosakis, Aj., Rosakis, P., Partition Of Plastic Work Into Heat And Stored Energy In Metals. Experimental Mechanics, 40 (2), 2000, 113-123.
[13] Gurson, A. L.: Continuum Theory of Ductile Rupture by Void Nucleation and Growth: Part I-Yield Criteria and Flow Rules for Porous Ductile Media, J. of Eng. Materials and Technology, 99(1977), S. 2-15.
[14] Nahshon, K., Hutchinson, J.W., Modification of the Gurson Model for shear failure, Euro. J. Mech. A/Solids, 2008, 27, 1-17.
[15] Gese, H., Werner, H., Hooputra, H., Dell, H., Heath, A., A comprehensive failure model for metallic structures in sheet metal forming and crash simulation, Europam, Paris, 11.–13. Oktober 2004.
[16] Bai, Y., Wierzbicki, T, Application of extended Mohr–Coulomb criterion to ductile fracture, Int J Fract (2010) 161,1–20.
[17] Taylor, G.I., Quinney, H., The latent energy remaining in a metal after cold working, Proceedings of the Royal Society of London, 143 (1934), 307–326.
[18] Queiroz, R.R.U, Cunha, F.G.G., Gonzalez, G.M., Study of dynamic strain aging in dual phase steel, Material Science and Engineering: A, Vol. 543 (2012), 84-87.
[19] Trondl, A., Klitschke, S., Böhme, W., Sun, D.-Z., Verformungs- und Versagensverhalten von Stählen für den Automobilbau unter crashartiger mehrachsiger Belastung, Fraunhofer IWM 2015 Schlussbericht, IWM-Berichts-Nr.: 1235/2015, Stiftungs-Nr. S24/10195/12.
[20] Klitschke, S., Böhme, W., Crashverhalten von Stählen im Automobilbau bei unterschiedlichen mehrachsigen Belastungen, Tagungsband Werkstoffprüfung 2014, S. 213-218.
[21] Klitschke, S., Böhme, W., Lienhard, J., Preußner, J., Schüler, J.,. Sköries, J., Charakterisierung der Werkstoffe HCT980X+Z110MB und HX340LAD unter crashartiger, mehrachsiger Belastung, AVIF-Projekt A278/VP979 (Stiftungs-Nr. S24/10195/12), Zwischenbericht PbA-Sitzung am 12.02.2014
[22] GOM, Technische Dokumentationen. Handbücher sowie verschiedene Artikel veröffentlicht durch GOM mbH. Braunschweig, Germany : s.n., 2010. Weitere Infos www.gom.com